Journal of Advanced Ceramics
2020, **9**(4): 481–492
https://doi.org/10.1007/s40145-020-0391-8

ISSN 2226-4108
CN 10-1154/TQ

Research Article

Theoretical prediction, synthesis, and crystal structure determination of new MAX phase compound V_2SnC

Qiang XU[a,†], Yanchun ZHOU[b,†], Haiming ZHANG[b,c], Anna JIANG[a], Quanzheng TAO[d], Jun LU[d], Johanna ROSÉN[d], Yunhui NIU[e], Salvatore GRASSO[a], Chunfeng HU[a,*]

[a]*Key Laboratory of Advanced Technologies of Materials*, *Ministry of Education*, *School of Materials Science and Engineering*, *Southwest Jiaotong University*, *Chengdu 610031*, *China*
[b]*Science and Technology on Advanced Functional Composite Laboratory*, *Aerospace Research Institute of Materials & Processing Technology*, *Beijing 100076*, *China*
[c]*School of Mechanical*, *Electronic and Control Engineering*, *Beijing Jiaotong University*, *Beijing 100044*, *China*
[d]*Thin Film Physics Division*, *Department of Physics*, *Chemistry*, *and Biology* (*IFM*), *Linköping University*, *Linköping SE-581 83*, *Sweden*
[e]*State Key Laboratory of Environment-friendly Energy Materials*, *Southwest University of Science and Technology*, *Mianyang 621010*, *China*

Received: December 25, 2019; Revised: May 12, 2020; Accepted: May 18, 2020

Abstract: Guided by the theoretical prediction, a new MAX phase V_2SnC was synthesized experimentally for the first time by reaction of V, Sn, and C mixtures at 1000 ℃. The chemical composition and crystal structure of this new compound were identified by the cross-check combination of first-principles calculations, X-ray diffraction (XRD), energy dispersive X-ray spectroscopy (EDS), and high resolution scanning transmission electron microscopy (HR-STEM). The stacking sequence of V_2C and Sn layers results in a crystal structure of space group $P6_3/mmc$. The *a*- and *c*-lattice parameters, which were determined by the Rietveld analysis of powder XRD pattern, are 0.2981(0) nm and 1.3470(6) nm, respectively. The atomic positions are V at 4f (1/3, 2/3, 0.0776(5)), Sn at 2d (2/3, 1/3, 1/4), and C at 2a (0, 0, 0). A new set of XRD data of V_2SnC was also obtained. Theoretical calculations suggest that this new compound is stable with negative formation energy and formation enthalpy, satisfied Born–Huang criteria of mechanical stability, and positive phonon branches over the Brillouin zone. It also has low shear deformation resistance c_{44} (second-order elastic constant, c_{ij}) and shear modulus (G), positive Cauchy pressure, and low Pugh's ratio (G/B = 0.500 < 0.571), which is regarded as a quasi-ductile MAX phase. The mechanism underpinning the quasi-ductility is associated with the presence of a metallic bond.

Keywords: V_2SnC; new MAX phase compound; crystal structure; first-principles calculations

† Qiang Xu and Yanchun Zhou contributed equally to this work.
* Corresponding author.
E-mail: chfhu@live.cn

1 Introduction

The layered machinable MAX phases are a large family of ternary carbides and nitrides with a general formula of $M_{n+1}AX_n$, where M is an early transition metal, A is a group of III_A or IV_A elements, X is carbon or nitrogen, and *n* is an integer, commonly equal to 1, 2, or 3 [1–3]. Structurally, the MAX phases can be regarded as alternatively stacking of transition metal carbide/nitride octahedra layers ($M_{n+1}X_n$) and A group element layers [4–7]. Depending on the value of *n*, the M_2AX, M_3AX_2, and M_4AX_3 phases are referred to be 211, 312, and 413 phases, respectively. As is known to all, the majority of the 211 phases (e.g., Cr_2AlC, originally called "*H*-phases") and two 312 phases (i.e., Ti_3SiC_2 and Ti_3GeC_2) were firstly reported by Nowtony *et al*. [8–10]. In 1999, the first 413 molecular composition, Ti_4AlN_3, was identified by Barsoum's group [11]. Since then the MAX phase family has grown quite rapidly [1–7]. Subsequently, the *n*-value is not limited to 3, other branches of the same family, such as 514, 615, and 716 phases $(Ti_{0.5}Nb_{0.5})_5AlC_4$ [4], Ta_6AlC_5 [6], and Ti_7SnC_6 [12] were determined. In addition to the conventional MAX phases mentioned above, there are several derivative MAX phases like $Ti_5Al_2C_3$, $Ti_5Si_2C_3$, and $Ti_7Si_2C_5$ have been observed in the thin-film or bulk samples [7,13]. It has come to light that these materials exhibit a unique combination of both ceramic-like and metal-like properties [1–7]. For example, like ceramics, they have low density, high strength and modulus, good corrosion, and high-temperature oxidation resistance; like metals, they are electrically conductive, relatively soft, readily machinable, resistant to thermal shock, and tolerant to damage [14,15]. Furthermore, these phases can be used as precursors for the two-dimensional (2D) materials MXenes by selectively etching out the group III_A or IV_A elements [16]. Recently, Mo_2Ga_2C, $Mo_2(Au_{1-x}Ga_x)_2C$, Ti_2Au_2C, and $Ti_3Au_2C_2$ with the double A-layer phases have been reported [17–20].

Considering these reported layered materials, new MAX phases and MAX phase-like compounds are still being synthesized and characterized [21–24]. Very recently, Sokol *et al*. [25] provided a comprehensive list of known MAX phases, bringing the total count to be 155. We note that some of important additions are the new ternary MAX phases: Mn_2GaC [26], Zr_2AlC [27], Nb_2GeC [28], Hf_3AlC_2 [29], and V_4AlC_3 [30]. The last phase, V_4AlC_3, which is the first and sole V-based ternary 413-type MAX phase so far, was identified by Hu *et al*. [30]. The other V-containing MAX phases have been identified mainly in the 211 class with Al, Ga, Ge, P, As, or Zn as A element [25,31]. There are few studies about in V–Sn–C system. Moreover, no ternary MAX phases have been so far synthesized in V–Sn–C system. Most recently, only a series of A layers multi-element magnetic solid solution MAX phases with general chemical formula $V_2(A_xSn_{1-x})C$ (A = Fe, Co, Ni, Mn, or their combinations) have been synthesized [32]. Due to the incorporation of one or more magnetic elements at the position A (Sn) of 211-type structure, these phases displayed ferromagnetic (FM) behavior. Also, considering the condition of formation, unlike M_3SnC_2 (M = Ti, Zr, Hf) MAX phases [33], the addition of these magnetic elements has no contribution to the formation of the initial and original MAX phase V_2SnC. Besides, Cover *et al.* [34] have comprehensively surveyed 240 M_2AX phases based on first-principles calculations in 2009, where the stability of V_2SnC was investigated and reported that this compound was intrinsically stable. Up to now, however, there is no experimental evidence for the existence of V_2SnC. Its crystal structure and a full set of XRD data remain unknown. Owing to the chemical similarity of constituent elements of MAX phases and considering the excellent electrical conductivity of other Sn-based MAX phases, such as Ti_2SnC ($14 \times 10^6\ \Omega^{-1}\cdot m^{-1}$) [35], the MAX phase V_2SnC might be potentially considered as electrical composites in reinforcement for metals and polymers.

In terms of the A element, Sn-containing MAX phases have received the most attention for two aspects: first, a recent study reports that Ti_2SnC shows efficient recovery mechanical damage by crack self-healing characteristics after the oxidation at low temperature and short period [36]. Second, Sn-based MAX phases, particularly in the 211-stoichiometry (M_2SnC, M = Ti, Zr, Hf, Nb), exhibit high electrical conductivity and stiffness, self-lubricity, and low hardness, which are promising as reinforcements for soft Cu to increase the strength and reduce the friction coefficient [12,35,36]. M_2SnC phases with Ti, Zr, Hf, Nb as M were firstly reported by Nowotny *et al*. [8–10] in the 1960s and 1970s. The properties of M_2SnC (M = Ti, Zr, Hf, Nb) bulk were investigated by Barsoum *et al*. [35] in the 1990s. They found that the electrical conductivities ranged from 2.4×10^6 to $14 \times 10^6\ \Omega^{-1}\cdot m^{-1}$, the hardness values were in the order of 3–5 GPa, and these

ceramics had graphite-like machinability. In order to raise the experiment to a theoretical level, Kanoun *et al.* [37] reported the theoretical study of properties of M_2SnC (M = Ti, Zr, Hf, Nb) by first-principles calculations. Considering the properties of MAX phases, elastic properties are of particular importance as they determine the macroscopic characteristics of the material, such as friction and machinability [1–7]. However, the experimental characterization of elastic properties is hindered by the production of pure samples. This makes theoretical research a necessary tool for understanding the material properties.

The purpose of this study is to explore the existence of V_2SnC and its crystal structure determination. Using a combination of first-principles calculations, X-ray diffraction (XRD), energy dispersive X-ray spectroscopy (EDS), and high resolution scanning transmission electron microscopy (HR-STEM), the lattice parameters and atomic positions were determined. We also report on the full XRD pattern data of V_2SnC for the first time. Furthermore, the stability and elastic properties of V_2SnC will also be presented and the mechanism for the quasi-ductility will be discussed based on electronic structure and chemical bonding analysis.

2 Theoretical and experimental details

2. 1 Theoretical calculation

Before experimental verification, the possible existence of V_2SnC was judged from the formation energy, formation enthalpy, elastic constants, and phonon dispersion curve. All the first-principles calculations were performed using the Cambridge Serial Total Energy Package (CASTEP) code [38]. The exchange-correlation energy was treated under generalized gradient approximation (GGA) [39]. The plane-wave basis set cutoff was 400 eV after convergent test and the special *k*-point sampling integration over the Brillouin zone was employed using the Monkhorst Pack method with 9 × 9 × 2 spatial *k*-point mesh [40]. Geometry optimization was achieved under the Broyden–Fletcher–Goldfarb–Shanno (BFGS) minimization scheme [41]. Lattice parameters and the atom positions are optimized until the total energy and maximum ionic displacement converged to 5×10^{-6} eV/atom and 5×10^{-4} Å, respectively. The calculations of the projected density of states were performed using a projection of the plane-wave electronic states onto a localized linear combination of atomic orbitals (LCAO) basis set.

The second-order elastic constants (c_{ij}) were determined from a linear fit of the calculated stress as a function of strain [42]. Four positive and four negative strains were applied for each strain component, with a maximum strain value of 0.3%. The criteria for convergence in optimizing atomic internal freedoms are: the difference on total energy within 5×10^{-6} eV/atom, the ionic Hellmann–Feynman forces within 0.002 eV/Å, and the maximum ionic displacement within 5×10^{-4} Å. The polycrystalline bulk modulus (B) and shear modulus (G) were calculated from the c_{ij} according to the Voigt, Reuss, and Hill approximations [43–45]. The phonon calculations were conducted with a finite displacement method.

2. 2 Material synthesis

The starting materials for the synthesis of V_2SnC are vanadium (99.9%, –300 mesh), tin (99.9%, –300 mesh), and graphite (99.9%, –300 mesh) powders. The powders were dryly-mixed in a V:Sn:C molar ratio of 2.0:1.1:1.0 in a resin jar for 24 h and sieved. Then the mixed powders were uniaxially pressed into a green compact using a steel die before putting into a graphite crucible. Reaction synthesis of V_2SnC was conducted in a tube furnace under flowing Ar atmosphere at 1000 ℃ for 2 h (MXG1400-60, Micro-X Corp., China). After naturally cooling down to ambient temperature, the as-prepared powders were immersed in a diluted hydrochloric acid solution (2 mol·L^{-1}, 200 mL) at room temperature for 10 h. Finally, the powders were washed in deionized water and dried in an oven.

Bulk V_2SnC was prepared by spark plasma sintering (SPS) of the powder compact at 1000 ℃ for 30 min under an applied pressure of 40 MPa in the Ar atmosphere (SPS-20T-10, Chenhua Corp., China). Thereafter, the surface contaminations of the dense sample were removed by using a grinding wheel.

2. 3 Crystal structure determination

Phase composition in V_2SnC powders and bulk were identified by using an X-ray diffractometer (Bruker D8 A25X, Karlsruhe, Germany) with incident Cu Kα radiation (λ = 1.54178 Å). The step size was 0.02° and the scanning rate was 2 (°)/min. The microstructure of V_2SnC was observed in a scanning electron microscope (FEI Inspect F50, USA) equipped with an energy dispersive spectrometer (Super Octane, USA). The stacking sequence of V_2C and Sn layers was directly

observed in a high resolution scanning transmission electron microscope (HR-STEM, FEI Titan3 60-300, FEI Co., the Netherlands) equipped with a high-angle annular dark-field (HAADF) detector. Rietveld refinement was performed by utilizing the FULLPROF software package [46]. Theoretical XRD pattern of V_2SnC was simulated using the Reflex powder diffraction code in the Accelrys Materials Studio program (Accelrys Inc., San Diego, USA). A full set of XRD patterns including reflection planes, peak positions, and intensities were obtained.

3 Results

3. 1 Theoretical calculation of V_2SnC

Figure 1 shows the crystal structure of V_2SnC, which is built by replacing Nb in Nb_2SnC [37] with V. After geometry optimization, the lattice constants and atom positions of the optimized structure are obtained, as listed in Table 1, which can be used as a reference for experimental investigations. For the possible existence evaluation, it can be justified from the formation energy, formation enthalpy, mechanical stability, and phonon dispersions over the Brillouin zone. The formation energy ($E_{\text{form}}(V_2SnC)$) can be determined from the total energy relative to the most stable polymorphic modifications of elements composing the compound.

$$2V + Sn + C \rightarrow V_2SnC \tag{1}$$

$$E_{\text{form}}(V_2SnC) = \frac{1}{2}E_{\text{tot}}(V_2SnC) - \left(2\times\frac{1}{2}E_{\text{tot}}(V) + \frac{1}{8}E_{\text{tot}}(Sn) + \frac{1}{4}E_{\text{tot}}(C)\right) \tag{2}$$

where E_{tot} is the total energy of the optimized structure of V_2SnC, V, Sn, and graphite. $E_{\text{form}}(V_2SnC)$ = –1.4834 eV < 0, indicating that V_2SnC is possibly stable under normal conditions.

The thermodynamic stability at ambient pressure concerning decomposition is quantified in terms of the formation enthalpy. Considering that the general reaction mechanism of MAX phases is the reaction between MX and A compounds by inserting A atoms into MX carbide/nitride crystal structure, the formation enthalpy of V_2SnC could be closely calculated by the following equation:

$$V_2C + Sn \rightarrow V_2SnC \tag{3}$$

$$\Delta H_{\text{form}}(V_2SnC) = H(V_2SnC) - H(Sn) - H(V_2C) \tag{4}$$

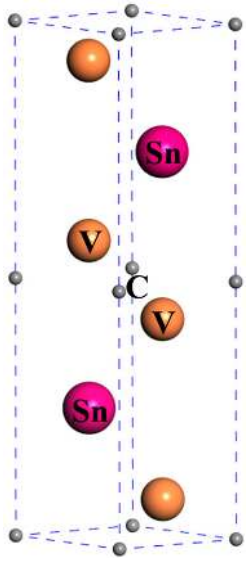

Fig. 1 Crystal structure of V_2SnC.

Table 1 Crystal structure parameters of V_2SnC

Formula	V_2SnC	
Crystal system	Hexagonal	
Space group	$P6_3/mmc$ (No. 194)	
Formula unit	$Z = 2$	
Crystal parameters	First-principles calculations	Rietveld refinement
Lattice constants (nm)	a = 0.3134	a = 0.2981(0)
	c = 1.2943	c = 1.3470(6)
Atomic positions	V 4f (1/3, 2/3, 0.0751)	V 4f (1/3, 2/3, 0.0776(5))
	Sn 2d (2/3, 1/3, 0.25)	Sn 2d (2/3, 1/3, 0.25)
	C 2a (0, 0, 0)	C 2a (0, 0, 0)

where $\Delta H_{\text{form}}(V_2SnC)$ is the formation enthalpy of V_2SnC. $H(V_2SnC)$, $H(Sn)$, and $H(V_2C)$ are the enthalpy of V_2SnC, Sn, and V_2C, respectively. The calculated $\Delta H_{\text{form}}(V_2SnC)$ is –0.0159 eV. The negative formation enthalpy indicates the possible existence of V_2SnC phase.

Additionally, the mechanical stability of V_2SnC was justified from the Born–Huang criteria [47]. For a hexagonal crystal, the conditions are expressed as

$$\begin{aligned} c_{44} &> 0 \\ c_{11} &> |c_{12}| \\ (c_{11} + 2c_{12})c_{33} &> 2c_{13}^2 \end{aligned} \tag{5}$$

Table 2 lists the c_{ij} of V_2SnC together with those of Ti_2SnC, Zr_2SnC, Hf_2SnC, Nb_2SnC, Cr_2AlC, and Ti_3SiC_2 [37,48,49]. It is seen that the stability conditions of V_2SnC are similar to those of MAX phases, demonstrating its stability under elastic strain perturbations.

Table 2 Theoretically predicted c_{ij}, bulk modulus (B), shear modulus (G), Young's modulus (E), Poisson's ratio (v), and Pugh's ratio (G/B) for V_2SnC, Ti_2SnC, Zr_2SnC, Hf_2SnC, Nb_2SnC, Cr_2AlC, and Ti_3SiC_2

Compound	c_{ij} (GPa)						B (GPa)	G (GPa)	E (GPa)	v	G/B
	c_{11}	c_{33}	c_{44}	c_{12}	c_{13}	c_{66}					
V_2SnC	336	304	85	126	122	105	190	95	244	0.286	0.500
Ti_2SnC [37]	337	329	169	86	102	126	176	138	328	0.188	0.784
Zr_2SnC [37]	269	290	148	80	107	94	157	110	268	0.215	0.700
Hf_2SnC [37]	330	292	167	54	126	138	173	132	316	0.195	0.763
Nb_2SnC [37]	341	321	183	106	169	118	209	126	314	0.250	0.603
Cr_2AlC [48,49]	385	360	154	94	118	132	188	140	346	0.210	0.718
Ti_3SiC_2 [48,49]	354	344	165	91	103	131	183	141	337	0.193	0.770

Besides, the stability of V_2SnC can also be judged from lattice dynamic investigations. As can be seen in the phonon dispersion and phonon density of state curves in Fig. 2, all phonon branches are positive, indicating the dynamical stability of this compound against mechanical perturbations.

3. 2 Synthesis of V_2SnC

In Section 3.1, V_2SnC is theoretically predicted as a possible stable compound. To experimentally verify the existence, V_2SnC was synthesized through the reaction of vanadium, tin, and graphite powders. Figure 3(a) shows the XRD pattern of as-prepared powders synthesized at 1000 ℃ for 2 h (the XRD pattern of bulk is the same). In Fig. 3(a), Sn, and $VC_{0.75}$ can be identified. In comparison with the simulated XRD pattern of V_2SnC in Fig. 3(b), which was generated using the Reflex powder diffraction code in Accelrys Materials Studio program, the peaks positioned at 13.174°, 26.517°, 40.277°, etc., which do not belong to either Sn or $VC_{0.75}$, coinciding with those

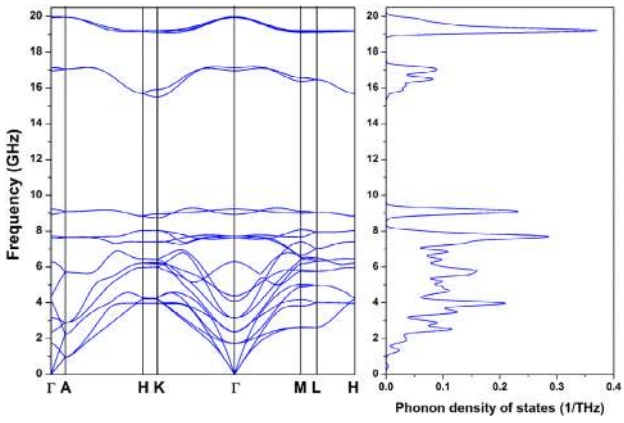

Fig. 2 Calculated phonon dispersion relations of V_2SnC.

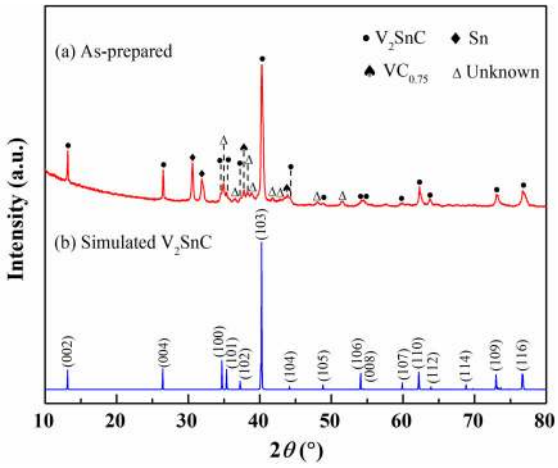

Fig. 3 Comparison between XRD patterns of (a) powders synthesized through the reaction between V, Sn, and C at 1000 ℃ for 2 h and (b) the simulated one of V_2SnC.

of V_2SnC in the simulated XRD pattern. Some small peaks, at ~34.934°, ~36.554°, ~51.553°, etc., remained unidentified (these unknown peaks are labeled on the pattern). This result demonstrates the presence of the new MAX phase V_2SnC. Since V_2SnC has not been synthesized in the experiment, the study of this new compound is intriguing.

It is well known that MAX phases crystallize in hexagonal structure and their grains are generally layered hexagons [1–7,50] in morphology. To confirm that V_2SnC has a similar microstructure, the microstructure of as-prepared powders and SPS sintered bulk was observed by SEM. As can be seen from Fig. 4(a) (high magnification on the right), V_2SnC exhibits the microstructure of typical thin hexagons. From the fracture surfaces of the bulk sample, lamellar microstructure features can clearly be observed, as shown in Figs. 4(b) and 4(c). To further

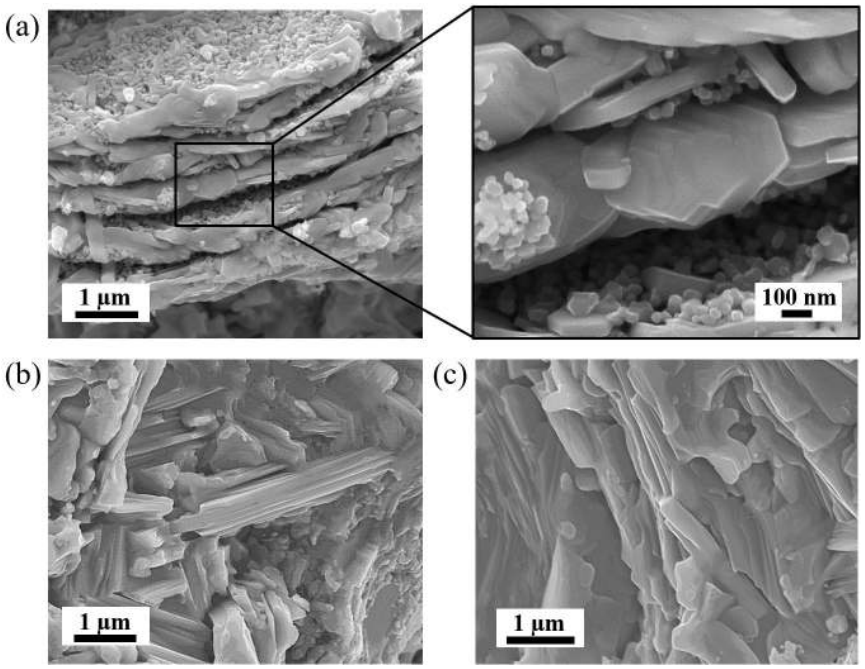

Fig. 4 Microstructure of (a) V_2SnC powders and (b, c) fracture surfaces of V_2SnC bulk fabricated by SPS.

identify the composition of this compound, the representative compositions from different grains and positions determined by EDS are listed in Table 3. Although EDS analysis is semi-quantitative and accurate determination of light elements like C is difficult, the nominal ratio of V:Sn:C can approximately be assumed to be 2:1:1. The above results further confirmed that the new MAX phase compound V_2SnC is experimentally existing.

3. 3 Determination of stacking sequence in V_2SnC

Previous studies demonstrated that the most efficient method to determine the stacking sequence in MAX phases is through STEM observation using *Z*-contrast image [4–6,51,52], wherein the stacking sequence of M and A layers can directly be revealed. Figure 5(a) presents a *Z*-contrast STEM image after fast Fourier transform (FFT) filtering, wherein the arrangement of the atoms on $(1\bar{1}00)$ plane is revealed. Two layers of V interleaved by one layer of Sn is obvious and the lattice constant in *c*-direction is 1.347 nm. Atom arrangement on $(11\bar{2}0)$ plane is shown in Fig. 5(b). Stacking sequences consisting of two layers of V interleaved by one layer of Sn are revealed, i.e., the stacking sequence of V and Sn follows A<u>B</u>AB<u>A</u>B similar to that of other M_2AC phases [51–53], i.e., every two layers of V atoms and one layer of Sn atoms are alternately stacked along the [0001] direction. The structure can also be regarded as a Sn layer inserted into the twin boundary of V_2C, as shown in the insert structure model in Fig. 5, similar to the other MAX phases [51–53]. The combination of XRD analysis, SEM, and STEM observation confirmed that the synthesized new phase is V_2SnC. The synthesis of the V_2SnC MAX phase is significant because it provides experimental evidence for the existence of this new compound, which opens the window to explore more M_2AX phases in other compositions. It also provides more opportunities for composition design and property control of MAX phases.

Table 3 Chemical compositions obtained from EDS analysis of V_2SnC grains

Point number	V (at%)	Sn (at%)	C (at%)	Atomic ratio (V:Sn:C)
1	48.01	22.99	29.00	2.09:1:1.44
2	46.00	22.14	31.86	2.08:1:1.44
3	45.86	23.02	31.11	1.99:1:1.35
4	46.58	22.58	30.84	2.06:1:1.35

3. 4 New set of XRD data of V_2SnC

XRD pattern is important for phase identification and structure analysis. Since the XRD pattern of V_2SnC is not available in the literature, it is useful to obtain a new set of patterns for this compound. To achieve such a goal, the Rietveld refinement of powder XRD pattern

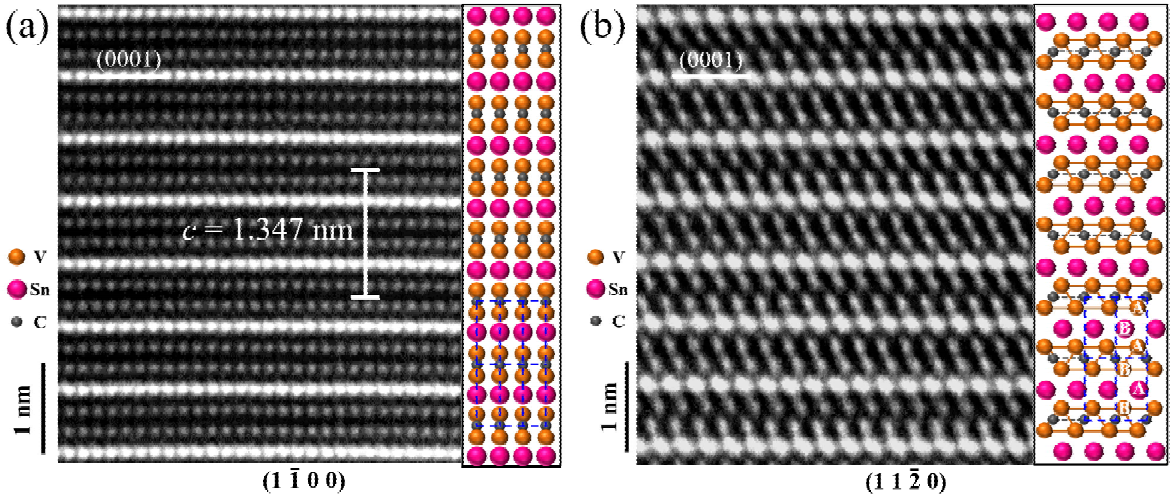

Fig. 5 *Z*-contrast STEM images of V_2SnC on (a) (1 $\bar{1}$00) and (b) (11$\bar{2}$0) planes. The insets are structure models representing the corresponding positions of V, Sn, and C atoms.

of V_2SnC was conducted at peak positions 2θ = 10°–80°. As shown in Fig. 6, the black crosses represent the experimental diffraction profile, while the red solid line denotes the theoretical pattern. The theoretical Bragg diffraction positions of V_2SnC, Sn, and $VC_{0.75}$ are marked vertical purple, green, and orange lines, respectively. The blue curve is the deviation between the calculated and experimental XRD patterns. The obtained reliability factors are R_p = 8.27% and R_{wp} = 12.34%, respectively, indicating good agreement between model and measured data. Detailed crystal structure information is depicted in Table 1. The space group of V_2SnC is $P6_3/mmc$ (No. 194) and the lattice constants are a = 0.2981(0) nm and c = 1.3470(6) nm. The atoms are located at: V 4f (1/3, 2/3, 0.0776(5)), Sn 2d (2/3, 1/3, 1/4), and C 2a (0, 0, 0). The difference between theoretical calculation and the Rietveld refinement is probably ascribed to the existence of defects in the crystal structure of V_2SnC. Besides, a new set of XRD data including Bragg diffraction planes (*hkl*), 2θ, interplane distance (d), and intensities (I) of V_2SnC are given in Table 4. These data are useful for phase identification and structural characterization of this new MAX phase V_2SnC.

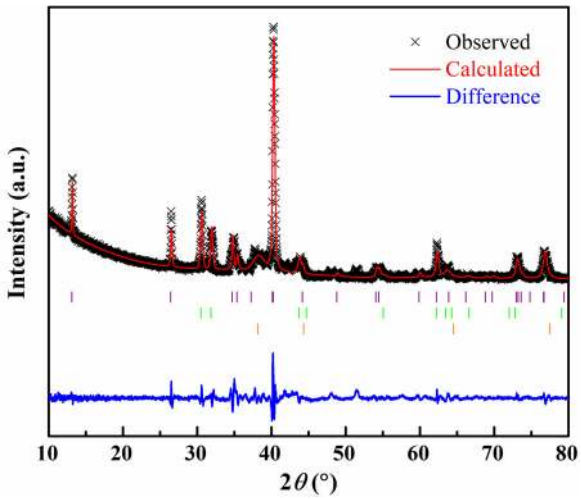

Fig. 6 Comparison between the observed (black crosses) and calculated XRD (red line) patterns of V_2SnC. The deviation plot (blue line) is shown in the lower part of Fig. 6. The purple, green, and orange ticks below the pattern represent the peak positions of the V_2SnC, Sn, and $VC_{0.75}$ phases, respectively.

4 Discussion

In Section 3, a new MAX phase V_2SnC was successfully synthesized for the first time. Its crystal structure was determined and a new set of XRD data was obtained. From the application point of view, it is intriguing to understand the specific properties of this compound, which allowed discussion on its elastic properties and mechanism that underpins these properties.

4. 1 Quasi-ductility judged from elastic properties

In Table 2, the elastic properties of V_2SnC are given, in which c_{11}, c_{33}, c_{44}, c_{12}, and c_{13} are independent, while c_{66} is not independent and is related to c_{11} and c_{12} through the following relationship:

$$c_{66} = 1/2(c_{11} - c_{12}) \quad (6)$$

Comparing the second-order elastic properties of

Table 4 Calculated and experimental data of reflections, 2θ, *d*-spacings, and intensities of V_2SnC. The peaks of (006), (201), (202), and (204) were not observed due to their low intensities

hkl	$2\theta_{Cal.}$ (°)	$2\theta_{Obs.}$ (°)	$d_{Cal.}$ (Å)	$d_{Obs.}$ (Å)	$I/I_{0Cal.}$ (%)	$I/I_{0Obs.}$ (%)
0 0 2	13.134	13.174	6.735	6.715	15.5	22.0
0 0 4	26.445	26.517	3.368	3.359	12.4	21.2
1 0 0	34.711	34.916	2.582	2.568	20.9	13.5
1 0 1	35.363	35.368	2.536	2.536	15.6	6.5
1 0 2	37.262	37.274	2.411	2.410	6.1	0.6
0 0 6	40.132	—	2.245	—	20.1	—
1 0 3	40.255	40.277	2.239	2.237	100.00	100.0
1 0 4	44.160	44.199	2.049	2.047	2.2	3.4
1 0 5	48.811	48.835	1.864	1.863	3.8	1.0
1 0 6	54.084	54.245	1.694	1.690	15.4	1.7
0 0 8	54.447	54.490	1.684	1.683	0.6	3.6
1 0 7	59.895	59.907	1.543	1.543	5.6	1.4
1 1 0	62.218	62.313	1.491	1.489	18.5	13.3
1 1 2	63.899	63.808	1.482	1.458	2.4	2.6
1 0 8	66.204	66.531	1.410	1.404	0.2	1.0
1 1 4	68.810	69.232	1.363	1.356	4.7	0.8
0 0 10	69.756	69.946	1.347	1.344	0.8	0.8
1 0 9	73.003	73.077	1.295	1.294	14.9	7.8
2 0 0	73.254	73.256	1.291	1.291	2.2	3.5
2 0 1	73.645	—	1.285	—	2.0	—
2 0 2	74.813	—	1.268	—	0.7	—
1 1 6	76.664	76.744	1.242	1.241	16.3	11.1
2 0 3	76.746	77.001	1.241	1.237	13.4	6.3
2 0 4	79.427	—	1.206	—	0.5	—

V_2SnC to those of Ti_2SnC, Zr_2SnC, Hf_2SnC, and Nb_2SnC, it is found that they have similar elastic constants c_{11}, c_{33}, c_{12}, and c_{13}. However, the shear deformation resistance c_{44} of V_2SnC (85 GPa) is much lower than those of Ti_2SnC (169 GPa), Zr_2SnC (148 GPa), Hf_2SnC (167 GPa), and Nb_2SnC (183 GPa) [37]. The c_{44} of V_2SnC is also lower than the well-investigated MAX phases of Cr_2AlC (154 GPa) and Ti_3SiC_2 (165 GPa) [48,49]. Low c_{44} indicates easy shear deformation along $[11\bar{2}0]$ |(0001). Low shear deformation of V_2SnC is also reflected from *G*, which represents the resistance to shape change of the polycrystalline material. The *G* of V_2SnC is 90 GPa, which is much lower than those of Ti_2SnC (138 GPa), Zr_2SnC (110 GPa), Hf_2SnC (132 GPa), Nb_2SnC (126 GPa), Cr_2AlC (140 GPa), and Ti_3SiC_2 (141 GPa) [37,48,49]. Low shear deformation is a characteristic of damage tolerant or quasi-ductile ceramics, which can also be judged from the Cauchy pressure and Pugh's shear to *G*/*B* [54]. For a hexagonal material, the Cauchy pressure is defined as: $P_a = c_{13} - c_{44}$, $P_c = c_{12} - c_{66}$. In general, a positive Cauchy pressure is an indication of ductile behavior. For this new MAX phase V_2SnC, Cauchy pressure is positive and in both *a* (P_a = +37 GPa) and *c* (P_c = +21 GPa) directions, indicating that V_2SnC is ductile in both *a*- and *c*-directions. Considering that the experimentally proved MAX phases like Ti_2SnC (P_a = –67 GPa, P_c = –40 GPa), Zr_2SnC (P_a = –41 GPa, P_c = –14 GPa), Hf_2SnC (P_a = –41 GPa, P_c = –84 GPa), Nb_2SnC (P_a = –14 GPa, P_c = –12 GPa), Cr_2AlC (P_a = –36 GPa, P_c = –38 GPa), and Ti_3SiC_2 (P_a = –62 GPa, P_c = –40 GPa) have negative Cauchy pressure, positive Cauchy pressure is the characteristic that distinguishes this new MAX phase V_2SnC from other MAX phases. Ductile behavior can also be judged from Pugh's shear to *G*/*B*. Low *G*/*B* (< 0.571) indicates intrinsic ductility. The *G*/*B* of V_2SnC is 0.500, which is lower than the criterion 0.571 and those of most MAX phases and MAX phase-like materials [2–7,50,55], revealing that V_2SnC is an intrinsic ductile MAX phase. Because there are no five independent slip systems for MAX phases, we still call this new MAX as quasi-ductile material.

4. 2 Mechanism of quasi-ductility

It has come to light that the elastic properties of MAX phases are underpinned by their electronic structure and chemical bonding. To gain more insight into the mechanism of the ductile behavior of this new MAX phase, the electronic structure of V_2SnC is investigated. Figure 7 shows the band structure of V_2SnC and the projected density of states of V, Sn, and C atoms. Similar to other MAX phases and MAX phase-like compounds [2–7,49,55], overlapping between valence and conduction bands across the Fermi level is clearly seen in H–K, K–Γ, and Γ–M directions in Fig. 7(a), revealing that V_2SnC is electrically conductive in both *a*–*b* plane and *c*-direction. However, the overlapping is anisotropic with less overlapping in H–K direction, indicating that the electrical conductivity is anisotropic. Overlapping between valence and conduction bands across the Fermi level also reveals the presence of metallic bonding, which is the origin of the quasi-ductility of V_2SnC. The difference of Cauchy pressure in *a*- and *c*-direction (P_a = +37 GPa and P_c = +21 GPa) can be attributed to the anisotropic metallic bonding.

As can be seen from Fig. 7(b), the main contribution to the electrical conductivity comes from V 3d states and Sn 5p states. In Figs. 7(c) and 7(d), it is seen that V 3d t_{2g} and V 3d e_g electrons mainly contribute to the electrical conductivity and there is minor contribution from Sn $5p_z$ electrons.

Easy shear deformation along $[11\bar{2}0]|(0001)$ can also be understood from the electronic structure and chemical bonding in V_2SnC. In Fig. 8(a), strong covalent-ionic V–C bond is formed through overlapping between V 3d t_{2g} and C $2p_x$ orbitals in the low energy range from –6 to –3 eV. In Fig. 8(b),

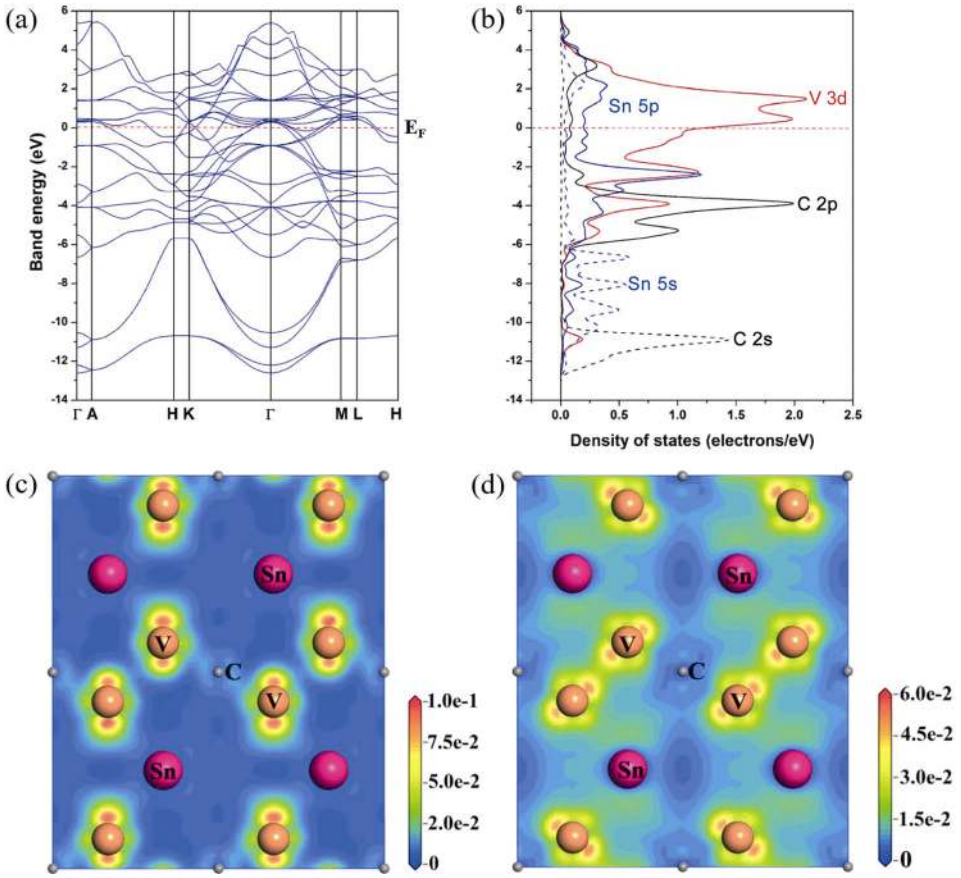

Fig. 7 (a) Band structure of V_2SnC; (b) projected density of V, Sn, and C atom states; (c, d) electron density maps on $(11\bar{2}0)$ plane of V_2SnC near Fermi level. V 3d e_g like, V 3d t_{2g} like, and Sn $5p_z$ like orbitals can be seen in Figs. 7(c) and 7(d), respectively. A 2 × 2 × 1 cell is used and the unit is electron/Å^3.

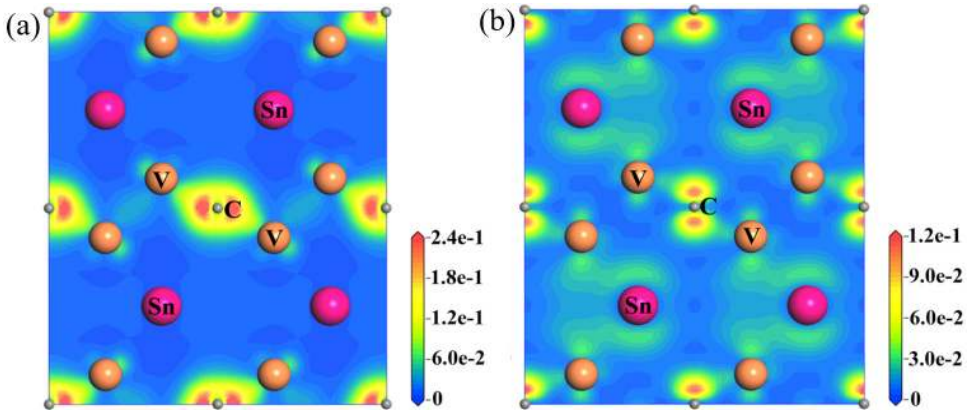

Fig. 8 Electron density maps on $(11\bar{2}0)$ plane of V_2SnC from (a) –6 to –3 eV and (b) –3 to –1 eV below the Fermi level, and the unit is electron/Å^3.

however, the interaction between V 3d e_g and Sn $5p_z$ orbitals is very weak and is metallic like in higher energy range from –3 to –1 eV. The weak V–Sn bonding can also be seen from the projected density of state curve in Fig. 7(b), wherein the V 3d and Sn 5p states are not overlapping although they are very close, demonstrating the weak interaction between them and the possible excellent quasi-plastic behavior.

5 Conclusions

In conclusion, the above results provide the existing evidence of MAX phase V_2SnC using theoretical prediction and experimental verification. Theoretically, the possible existence of this compound was predicted from the negative formation energy and formation enthalpy, satisfied Born–Huang criteria of mechanical stability, and positive dispersions of all phonon branches over the Brillouin zone. Experimentally, this new MAX phase was synthesized for the first time by heating the V, Sn, and C starting powder mixture at 1000 ℃. V_2SnC exhibits a typical laminar microstructure similar to other MAX phases. The V_2C and Sn layers are alternatively stacked along the [0001] direction. The lattice parameters are a = 0.2981(0) nm and c = 1.3470(6) nm, and the atomic positions are V 4f (1/3, 2/3, 0.0776(5)), Sn 2d (2/3, 1/3, 1/4), and C 2a (0, 0, 0). Also, a new set of XRD data of V_2SnC was obtained, which is useful for further phase identification and structure analysis. First-principles calculations indicated that this new MAX phase of V_2SnC has low shear deformation resistance c_{44} and G, positive Cauchy pressure, and low G/B = 0.500 < 0.571, which could be judged as a quasi-ductile ceramic. The mechanism underpinning the quasi-ductility is the presence of metallic bond, dominated by the V 3d electrons near the Fermi level as well as the contribution of Sn 5p electrons.

Acknowledgements

This study is supported by Thousand Talents Program of Sichuan Province, the Open Project of State Key Laboratory Cultivation Base for Nonmetal Composites and Functional Materials (17kffk01), Outstanding Young Scientific and Technical Talents in Sichuan Province (2019JDJQ0009), and the National Natural Science Foundation of China (No. 51741208).

References

[1] Barsoum MW. The $M_{N+1}A_N$ phases: A new class of solids; thermodynamically stable nanolaminates. *Prog Solid State Chem* 2000, **28**: 201–281.

[2] Wang JY, Zhou YC. Recent progress in theoretical prediction, preparation, and characterization of layered ternary transition-metal carbides. *Annu Rev Mater Res* 2009, **39**: 415–443.

[3] Wang XH, Zhou YC. Layered machinable and electrically conductive Ti_2AlC and Ti_3AlC_2 ceramics: A review. *J Mater Sci Technol* 2010, **26**: 385–416.

[4] Zheng LY, Wang JM, Lu XP, *et al*. $(Ti_{0.5}Nb_{0.5})_5AlC_4$: A new-layered compound belonging to MAX phases. *J Am Ceram Soc* 2010, **93**: 3068–3071.

[5] Lin ZJ, Zhuo MJ, Zhou YC, *et al*. Structural characterization of a new layered-ternary Ta_4AlC_3 ceramic. *J Mater Res* 2006, **21**: 2587–2592.

[6] Lin ZJ, Zhuo MJ, Zhou YC, *et al*. Microstructures and theoretical bulk modulus of layered ternary tantalum aluminum carbides. *J Am Ceram Soc* 2006, **89**: 3765–3769.

[7] Zhang H, Wang XH, Ma YH, *et al*. Crystal structure determination of nanolaminated $Ti_5Al_2C_3$ by combined techniques of XRPD, TEM and *ab initio* calculations. *J Adv Ceram* 2012, **1**: 268–273.

[8] Nowotny VH. Strukturchemie einiger Verbindungen der Übergangsmetalle mit den elementen C, Si, Ge, Sn. *Prog Solid State Chem* 1971, **5**: 27–70.

[9] Jeitschko W, Nowotny H, Benesovsky F. Carbides of formula T_2MC. *J Less Common Met* 1964, **7**: 133–138.

[10] Jeitschko W, Nowotny H, Benesovsky F. Ti_2AlN, eine stickstoffhaltige H-Phase. *Monatshefte Für Chemie* 1963, **94**: 1198–1200.

[11] Barsoum MW, Farber L, Levin I, *et al.* High-resolution transmission electron microscopy of Ti_4AlN_3, or $Ti_3Al_2N_2$ revisited. *J Am Ceram Soc* 1999, **82**: 2545–2547.

[12] Zhang J, Liu B, Wang JY, *et al*. Low-temperature instability of Ti_2SnC: A combined transmission electron microscopy, differential scanning calorimetry, and X-ray diffraction investigations. *J Mater Res* 2009, **24**: 39–49.

[13] Palmquist JP, Li S, Persson POÅ, *et al*. $M_{n+1}AX_n$ phases in the Ti–Si–C system studied by thin-film synthesis and *ab initio* calculations. *Phys Rev B* 2004, **70**: 165401–165413.

[14] Zhou YC, Sun ZM. Micro-scale plastic deformation of polycrystalline Ti_3SiC_2 under room-temperature compression. *J Eur Ceram Soc* 2001, **21**: 1007–1011.

[15] Barsoum MW, El-Raghy T. Synthesis and characterization of a remarkable ceramic: Ti_3SiC_2. *J Am Ceram Soc* 1996, **79**: 1953–1956.

[16] Naguib M, Mashtalir O, Carle J, *et al*. Two-dimensional transition metal carbides. *ACS Nano* 2012, **6**: 1322–1331.

[17] Hu C, Lai CC, Tao Q, *et al*. Mo_2Ga_2C: a new ternary nanolaminated carbide. *Chem Commun* 2015, **51**: 6560–6563.

[18] Lai C, Fashandi H, Lu J, *et al*. Phase formation of

nanolaminated Mo_2AuC and $Mo_2(Au_{1-x}Ga_x)_2C$ by a substitutional reaction within Au-capped Mo_2GaC and Mo_2Ga_2C thin films. *Nanoscale* 2017, **9**: 17681–17687.

[19] Fashandi H, Lai C, Dahlqvist M, *et al*. Ti_2Au_2C and $Ti_3Au_2C_2$ formed by solid state reaction of gold with Ti_2AlC and Ti_3AlC_2. *Chem Commun* 2017, **53**: 9554–9557.

[20] Fashandi H, Dahlqvist M, Lu J, *et al*. Synthesis of Ti_3AuC_2, $Ti_3Au_2C_2$ and Ti_3IrC_2 by noble metal substitution reaction in Ti_3SiC_2 for high-temperature-stable ohmic contacts to SiC. *Nat Mater* 2017, **16**: 814–819.

[21] Hu CF, Li FZ, Zhang J, *et al*. Nb_4AlC_3: A new compound belonging to the MAX phases. *Scripta Mater* 2007, **57**: 893–896.

[22] Zhou YC, Meng FL, Zhang J. New MAX-phase compounds in the V–Cr–Al–C system. *J Am Ceram Soc* 2008, **91**: 1357–1360.

[23] Zhang HM, Dai FZ, Xiang HM, *et al*. Crystal structure of Cr_4AlB_4: A new MAB phase compound discovered in Cr–Al–B system. *J Mater Sci Technol* 2019, **35**: 530–534.

[24] Zhou YC, Xiang HM, Zhang HM, *et al*. Theoretical prediction on the stability, electronic structure, room and elevated temperature properties of a new MAB phase Mo_2AlB_2. *J Mater Sci Technol* 2019, **35**: 2926–2934.

[25] Sokol M, Natu V, Kota S, *et al*. On the chemical diversity of the MAX phases. *Trends Chem* 2019, **1**: 210–223.

[26] Ingason AS, Petruhins A, Dahlqvist M, *et al*. A nanolaminated magnetic phase: Mn_2GaC. *Mater Res Lett* 2014, **2**: 89–93.

[27] Lapauw T, Lambrinou K, Cabioc'h T, *et al*. Synthesis of the new MAX phase Zr_2AlC. *J Eur Ceram Soc* 2016, **36**: 1847–1853.

[28] Eklund P, Dahlqvist M, Tengstrand O, *et al*. Discovery of the ternary nanolaminated compound Nb_2GeC by a systematic theoretical-experimental approach. *Phys Rev Lett* 2012, **109**: 035502.

[29] Lapauw T, Tunca B, Cabioch T, *et al*. Synthesis of MAX phases in the Hf–Al–C system. *Inorg Chem* 2016, **55**: 10922–10927.

[30] Hu CF, Zhang J, Wang JM, *et al*. Crystal structure of V_4AlC_3: A new layered ternary carbide. *J Am Ceram Soc* 2008, **91**636-639

[31] Li M, Lu J, Luo K, *et al*. Element replacement approach by reaction with Lewis acidic molten salts to synthesize nanolaminated MAX phases and MXenes. *J Am Chem Soc* 2019, **141**: 4730–4737.

[32] Li YB, Lu J, Li M, *et al*. Multielemental single–atom-thick A layers in nanolaminated $V_2(Sn,A)C$ (A = Fe, Co, Ni, Mn) for tailoring magnetic properties. *PNAS* 2020, **117**: 820–825.

[33] Lapauw T, Tunca B, Cabioc'h T, *et al*. Reactive spark plasma sintering of Ti_3SnC_2, Zr_3SnC_2 and Hf_3SnC_2 using Fe, Co or Ni additives. *J Eur Ceram Soc* 2017, **37**: 4539–4545.

[34] Cover MF, Warschkow O, Bilek MM, *et al*. A comprehensive survey of M_2AX phase elastic properties. *J Phys: Condens Matter* 2009, **21**: 305403.

[35] Barsoum MW, Yaroschuk G, Tyagi S. Fabrication and characterization of M_2SnC (M = Ti, Zr, Hf and Nb). *Scripta Mater* 1997, **37**: 1583–1591.

[36] Li SB, Bei GP, Chen XD, *et al*. Crack healing induced electrical and mechanical properties recovery in a Ti_2SnC ceramic. *J Eur Ceram Soc* 2016, **36**: 25–32.

[37] Kanoun MB, Goumri-Said S, Reshak AH. Theoretical study of mechanical, electronic, chemical bonding and optical properties of Ti_2SnC, Zr_2SnC, Hf_2SnC and Nb_2SnC. *Comput Mater Sci* 2009, **47**: 491–500.

[38] Clark SJ, Segall MD, Pickard CJ, *et al*. First principles methods using CASTEP. *Zeitschrift Für Kristallographie-Cryst Mater* 2005, **220**: 567–570.

[39] Perdew JP, Burke K, Ernzerhof M. Generalized gradient approximation made simple. *Phys Rev Lett* 1996, **77**: 3865–3868.

[40] Chadi DJ. Special points for Brillouin-zone integrations. *Phys Rev B* 1977, **16**: 1746–1747.

[41] Pfrommer BG, Côté M, Louie SG, *et al*. Relaxation of crystals with the quasi-Newton method. *J Comput Phys* 1997, **131**: 233–240.

[42] Ravindran P, Fast L, Korzhavyi PA, *et al*. Density functional theory for calculation of elastic properties of orthorhombic crystals: Application to $TiSi_2$. *J Appl Phys* 1998, **84**: 4891–4904.

[43] Voigt W. *Lehrbuch der Kristallphysik*. New York: Macmillan, 1928. (in German)

[44] Reuss A. Berechnung der Fließgrenze von Mischkristallen auf Grund der Plastizitätsbedingung für Einkristalle. *ZAMM-J Appl Math Mech/Zeitschrift Für Angewandte Math Und Mech* 1929, **9**: 49–58.

[45] Hill R. The elastic behaviour of a crystalline aggregate. *Proc Phys Soc A* 1952, **65**: 349–354.

[46] Rodríguez-Carvajal J. Recent advances in magnetic structure determination by neutron powder diffraction. *Phys B: Condens Matter* 1993, **192**: 55–69.

[47] Born M, Huang K. *Dynamical Theory of Crystal Lattices*. Oxford (UK): Oxford University Press, 1954.

[48] Zhou YC, Xiang HM, Dai FZ, *et al*. Cr_5Si_3B and Hf_5Si_3B: New MAB phases with anisotropic electrical, mechanical properties and damage tolerance. *J Mater Sci Technol* 2018, **34**: 1441–1448.

[49] Zhou YC, Xiang HM, Dai FZ. Y_5Si3C and $Y_3Si_2C_2$: Theoretically predicted MAX phase like damage tolerant ceramics and promising interphase materials for SiC_f/SiC composites. *J Mater Sci Technol* 2019, **35**: 313–322.

[50] Zhou YC, Dong HY, Wang XH, *et al*. Preparation of Ti_2SnC by solid–liquid reaction synthesis and simultaneous densification method. *Mater Res Innov* 2002, **6**: 219–225.

[51] Lin ZJ, Zhuo M, Zhou YC, *et al*. Atomic scale characterization of layered ternary Cr_2AlC ceramic. *J Appl Phys* 2006, **99**: 076109.

[52] Bentzel GW, Naguib M, Lane NJ, *et al*. High-temperature neutron diffraction, Raman spectroscopy, and first-

principles calculations of Ti_3SnC_2 and Ti_2SnC. *J Am Ceram Soc* 2016, **99**: 2233–2242.

[53] Lin ZJ, Li MS, Zhou YC. TEM investigations on layered ternary ceramics. *J Mater Sci Technol* 2007, **23**: 145–165.

[54] Pugh SF. XCII. Relations between the elastic moduli and the plastic properties of polycrystalline pure metals. *Lond Edinb Dublin Philos Mag J Sci* 1954, **45**: 823–843.

[55] Zhou YC, Xiang HM, Dai FZ, *et al*. $Y_5Si_2B_8$: A theoretically predicted new damage-tolerant MAB phase with layered crystal structure. *J Am Ceram Soc* 2018, **101**: 2459–2470.